THE JOURNAL OF PHYSICAL CHEMISTRY B

ARTICLE

pubs.acs.org/JPCB

Environmental Effects on the Lignin Model Monomer, Vanillyl Alcohol, Studied by Raman Spectroscopy

Kiki L. Larsen and Søren Barsberg*

Faculty of Life Sciences, University of Copenhagen, Rolighedsvej 23, DK-1958 Frederiksberg C, Denmark

ABSTRACT: Structural analysis of plant materials, i.e., lignin, cellulose, hemicellulose, etc., supports the growing interest of their uses, e.g., as sources for biofuels or materials. Lignin is a main polymer formed from three phenolic presursors, containing none, one, or two OMe groups, i.e., H, G, and S units, respectively. Raman spectroscopy gives valuable knowledge on lignin and has a large potential for further developments. Thus in the present work we show how the use of electronic structure theory can support the study of environmental effects on lignin Raman bands. Raman spectra of the lignin model monomer, vanillyl alcohol (G type), dissolved in different solvents were compared to investigate such effects on the Raman band shapes and positions. Density functional theory combined with the polarizable continuum model were applied to assign the observed bands and tested for prediction accuracy. Two ring deformation modes at ∼1600 cm^{-1} showed strong dependency on solvent ability to act as hydrogen bond donor, and this has to be considered in addition to substitutional effects on these modes.

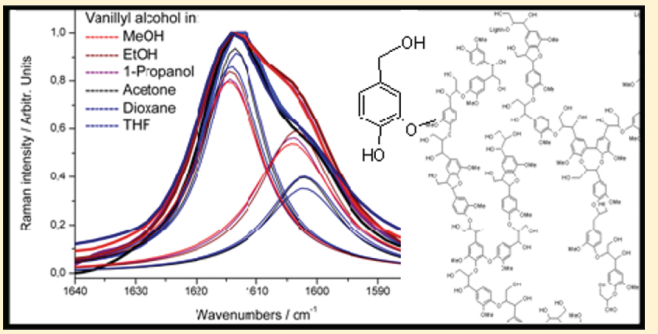

INTRODUCTION

Lignin is the second most abundant plant polymer on earth.[1] Together with cellulose and hemicellulose it represents the most abundant polymers making up wood and plants. Lignin varies in terms of linkage types, substitution patterns, between plant species, between cell types within a single plant, and between different parts of the wall of a single cell. Its chemical and physical structure is highly complex and irregular, and in order to describe it, statistics are required (e.g., distribution of monomer and linkage types).[2] Lignins are traditionally considered to be dehydrogenative polymers formed from three monolignol precursors: *p*-coumaryl alcohol, coniferyl alcohol, and sinapyl alcohol. Figure 1 illustrates a tentative lignin structure and the three monolignols.[3]

The monolignols are distinguishing by methoxy group substitutions, i.e., coumaryl alcohol (H: 4-hydroxycinnamyl alcohol), coniferyl alcohol (G: 4-hydroxy-3-methoxycinnamyl alcohol), and sinapyl alcohol (S: 4-hydroxy-3,5-dimethoxycinnamyl alcohol) moieties. The aromatic interconnected units resulting from these are (when incorporated into the lignin polymer) called *p*-hydroxyphenyl (H), guaiacyl (G), and syringyl (S) units, and in the following these terms are referred to in abbreviated form as H units, G units, and S units.

Raman spectroscopy is a useful vibrational spectroscopic tool in the investigations of the chemical components of wood and plant materials and especially lignin, because no sample preparation is needed and it therefore provides in situ information on the cell wall and its chemical components. It provides a powerful method of detecting the lignin chemical structure and the modifications of this.[4,5] The assignment of lignin Raman bands supports the crucial link between experimental data and structural knowledge, i.e., the "how" of how to get from data to knowledge.

Here a specific issue is how substitution influences lignin Raman spectra? This issue can, however, only be appropriately addressed if the influence of environment on lignin Raman spectra is examined. Thus any structural part of lignin can in principle interact noncovalently with proximate lignin structures or other cell wall components. These interactions may span from weak, e.g., van der Waal, to stronger hydrogen bonding interactions. This results in positional and intensity shifts of Raman bands, and in the present work we examine the magnitude of such shifts and their relative importance compared with substitutional shifts, e.g., H → G → S, of lignin structure. For this purpose a G unit phenolic lignin model, vanillyl alcohol, was chosen as a representative of a common lignin substructure.

Fourier transform Raman technique (NIR-FT) uses a NIR laser source with a photon energy well below troublesome low energy electronic transitions of lignin. By applying this method good quality spectra relatively free of fluorescence interference from various lignin-containing materials can be obtained.[6−9] Today also more sophisticated Raman spectroscopic methods can overcome this problem.[10−12] UV resonance Raman spectroscopy exploits the combined benefit of the resonantly enhanced Raman signal and the usually relatively much longer wavelengths of fluorescence emission compared to Raman photons.[11−13] For laser lines positioned in the visible part of the spectrum, the Raman photons occur in an energy range coinciding with lignin laser-induced fluorescence and the challenge is then to detect and separate the relatively very weak Raman signals from the

Received: April 27, 2011
Revised: August 8, 2011
Published: August 10, 2011

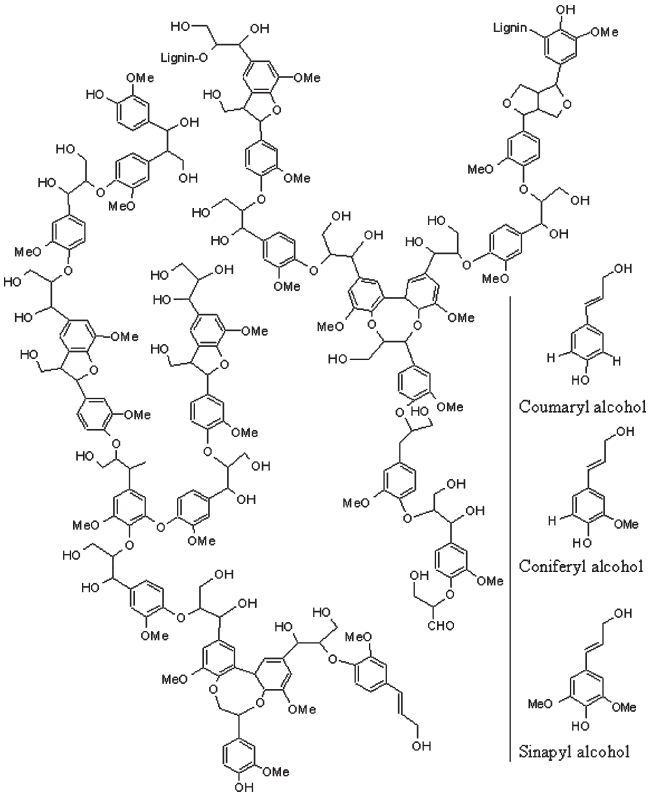

Figure 1. Tentative lignin structure reproduced from ref 3 and the three monolignols.

fluorescence background. Kerr gated Raman spectroscopy[10,14−16] exploits the different time-domain characteristics of fluorescence and Raman emission by allowing the detector to see only a narrow ps time-domain window centered on the excitation laser pulse.[11,12,17] Hereby the relative strength of the Raman signal is significantly increased since the fluorescence usually occurs on the ns time scale leaving a small fraction of it to be detected within the ps window. The Raman signal itself can also be enhanced several orders of magnitude by surface enhanced raman spectroscopy (SERS). This method exploits the change in Raman polarizability tensor of the material or compound of interest due to a formation of a complex between this and a roughened metal surface, usually gold or silver.[18,19] Convincing developments have thus been experienced within the area of Raman spectroscopy of lignin. However, this has not been complemented from a theoretical side. The advent of density functional theory (DFT)[20,21] and its extensive practical advantage has enabled a more reliable prediction of vibrational bands and not the least their associated intensities, which is not based on empirical data (apart from the parametrization of functionals) but on first principles, i.e., basic electronic structure theory. The introduction of the B3LYP density functional[22−25] has played a decisive role in this respect, and it is known to perform well for vibrational properties. The solvent effect, e.g., the effect of noncovalent interactions with proximate structures, was modeled by the polarizable continuum model (PCM) as invented by Tomasi and co-workers and implemented in the Gaussian software package.[26] The PCM is fully integrated with the B3LYP calculation of electronic density and charges and is thus able to predict the influence of proximate structures or environment on the vibrations and Raman intensities of the compound of interest.

Inclusion of explicit solvent molecules in the studies of biomolecules offers another route (which may be combined with the PCM) to investigate the solvent effect on for example Raman optical activities. Such studies have been undertaken by, e.g., Jalkanen,[27−29] Frimand,[30] Tajkhorshid,[31] and Deng.[32]

However, the combination of electronic structure DFT-PCM calculations and Raman spectroscopy has been used to study the lignin model monomer, vanillyl alcohol, to obtain fundamental information on its vibrational behavior when changing its environment. The information thus obtained is a necessary prerequisite for a proper understanding of the role of substitution as well as environment on the vibrational Raman spectra of lignin structures. Even though this model compound is not representative for all structural elements of lignin, it will serve to make the principal complexities in interpreting and assigning lignin Raman spectra more apparent for the scientific community and thus contribute to develop this exciting and promising field further. More accurate methods than the broadly accepted DFT-PCM with regard to investigating solvent effects exist, but with our purpose of assigning vibrations giving rise to Raman bands and using this information to account for solvent induced changes, the DFT PCM B3LYP method serves well as a compromise between accuracy and computational feasibility, and its performance for lignin structures has not been examined before.

EXPERIMENTAL METHODS

Chemicals. The solute 4-hydroxy-3-methoxy-benzyl alcohol (vanillyl alcohol, VA) and the solvents ethanol (EtOH), methanol (MeOH), 1-propanol (PrOH), acetone (Ace), tetrahydrofuran (THF), and dioxane (Diox) were obtained from Sigma-Aldrich and recrystallized or distilled prior to use.

Samples. VA was dissolved in the solvents in a number of different w/w % ratios and the largest possible ratio chosen. For all solvents no wavenumber shifts of Raman bands occurred as a function of concentration whereby the following concentrations of VA were used: EtOH, 14%; MeOH, 30%; PrOH, 6%; Ace, 10%; THF, 15%; and Diox, 20%. The solutions were transferred to standard electron spin resonance (ESR) 2 mm inner diameter glass tubes, which were sealed and used in the Raman spectrometer.

The six solvents were chosen considering the variation of their dielectrical constant (K) as well as their ability to function as a hydrogen donor and/or electron donor. The solvents EtOH (K = 24.6), MeOH (K = 32.6), and PrOH (K = 20.5) have the ability to act as both hydrogen (H) bond donor and acceptor, whereas Ace (K = 20.5), THF (K = 7.4), and Diox (K = 2.3) only function as H bond acceptors.

Raman Spectroscopy. Spectra were obtained using a Bruker RFS 100 FT-Raman spectrometer. The laser used was a Nd:YAG laser at 1064 nm (280 mW), and the spectral resolution was 4 cm^{-1}. The wavenumbers were calibrated using the characteristic band positions of cyclohexane[33] which is a recommended frequency standard.[34] The CH- and OH-stretching (ν_{CH} and ν_{OH}) regions >2000 cm^{-1} have been disregarded in this study, partly because instrumental cut off at 3500 cm^{-1} hinders complete information on the hydrogen bonding state (as revealed by the ν_{OH} bands expected above 3100 cm^{-1}) and partly because the sp^2 and sp^3 hybridized ν_{CH} area (3100−2800 cm^{-1}) is dominated by intense solvent bands which makes it difficult to obtain reliable data. Thus, only the spectral interval 1800−300 cm^{-1} is considered.

Spectral Manipulation. The procedures described in the following were followed by use of the Microcal OriginPro (ver. 7.5) software. The spectra were corrected by subtracting an appropriately scaled spectrum of the solvent. The scaling constants were chosen so the following bands were best removed: EtOH, 883 cm^{-1}; MeOH, 1033 cm^{-1}; PrOH, 858 cm^{-1}; Ace, 786 cm^{-1}; THF, 914 cm^{-1}; and Diox, 1014 cm^{-1}. Two criteria were used when choosing these bands: (a) a high Raman intensity and (b) no overlap with solute bands. After subtraction of the solvent spectrum, the spectra were divided into the following intervals: 1800−1550, 1550−1500, 1500−1050, 1050−850, 850−650, and 650−300 cm^{-1}. The intervals were chosen so that no VA band was positioned on an interval border. For each interval a straight baseline was subtracted from the spectrum. Band fitting was performed by Lorentzian band shapes, that showed a better fit to the line shapes than using a Gaussian band shape, and bands from solvent subtraction artifacts were disregarded. These artifacts occur if the pure solvent vibrational bands and the solvent part of solute/solvent solution bands are not completely overlapping. The solvent subtracted and Lorentz fitted spectra were combined and displayed using the intervals 1700−950 and 950−300 cm^{-1}.

Simulation of Raman Spectra. Harmonic vibrational frequencies and Raman intensities were calculated for VA in the solvents THF, Ace, EtOH, and MeOH using the G03 software package.[26] For this purpose the implicit solvation model PCM was used with its default settings (e.g., UA0 for atomic radii definitions). This version did not allow for the use of dioxane or 1-propanol as solvent models. Vibrations were visualized by the Gausview software, which was also used to generate simulated spectra (by convolution of a 4 cm^{-1} width Lorentzian band shape (fwhm) with predicted positions/intensities).[26] For harmonic frequencies and Raman intensities, the B3LYP functional was used with the 6-31+G(d) basis set and "tight" geometry convergence ($<10^{-6}$ au root mean square (rms) force, $<4 \times 10^{-6}$ au rms displacement), "tight" self-consistent field (SCF) convergence ($<10^{-8}$ au rms density matrix), and the "ultrafine" integration grid (i.e., 99 radial shells and 590 angular points).

The vibrational properties of VA in a specific model solvent were predicted within the PCM for each conformer A, B, and C (see the Results section for an elaboration of conformations) and then obtained as a weighted average of these. However, not all PCM/B3LYP structural (geometry) optimizations could converge within the chosen convergence criteria, and if convergence was achieved the first frequency was often negative.

This was not resolved by increasing the optimization cycle numbers >50 as the energy would always fluctuate between two close levels presumably caused by instability of the PCM tessellation procedure. Hence for these problematic cases only 50 cycles were allowed, and from these the three lowest energy intermediate structures were chosen (and not further optimized), all obeying rms gradient $<10^{-4}$ au rms force and $<1.6 \times 10^{-2}$ au rms displacement, and they were then each subjected to a frequency calculation. The soundness of this procedure was confirmed by the fact that the three sets of vibrational data were always practically identical, even if separated by several cycles, i.e., the oscillations were limited to the very lowest frequency modes, whereas higher frequency modes relevant for the present work were converged.

Some of the structures gave a negative frequency but only for the first normal mode (lowest frequency) corresponding to a rotation of the entire CH_2OH in VA, i.e., changing the $C_2-C_3-C_4-C_7$ dihedral angle (see Figure 3). The potential energy surface (PES) as a function of this angle is relatively flat. The system is thus easily trapped in a local saddle point along the (rotational) coordinate corresponding to the first normal mode vibration. This was overcome by allowing the (unconstrained) optimizations to start from slightly (few degrees) different predefined $C_2-C_3-C_4-C_7$ angles in order to target the genuine local minimum for which a subsequent frequency calculation then produced no negative frequencies.

RESULTS

Experimental Raman Spectra. To investigate the solvents effect on VA bands, the band center wavenumbers, ω_C, intensities, I, and the Full width half maximum (fwhm) were obtained by fitting Lorentzian band shapes to the observed bands. The intensities were normalized with respect to the intensity of the band at ~1614 cm^{-1}, giving I_N. The ω_C, I_N, and fwhm for the experimental data are displayed in Table 1. Low intensity bands produce less reliable band data. Therefore only bands of intensities >0.14 are considered in this study.

In Table 2, the average is taken for the center band positions for the VA bands in alcohol solvents and the nonalcohol solvents. The standard deviation (STD) has been calculated using

$$\hat{\sigma} = \mathrm{STD} = \sqrt{\frac{1}{n-1}\sum_{i=1}^{n}(x_i - \bar{x})^2}$$

For the intensities the STD has been calculated in percentage to the normalized band at 1615 cm^{-1}. Also, the difference between the average values in the two types of solvents is displayed.

fwhm is known to be a noticeable parameter characterizing interactions like hydrogen bonding since band shapes are very dependent on the surrounding solvent molecules. When looking at Table 2, the vibrations showing the largest shifts are #A, #C, and #I−K. Vibration #A narrowed ~2 cm^{-1} when changing the solvent from alcoholic, which can function as hydrogen and electron donors, to non-alcoholic, which can only function as electron donors. The largest change in fwhm was from vibration #C which narrowed by ~4 cm^{-1}. Vibration #J broadened by ~3 cm^{-1}. The fwhm for vibrations #I and #K are, though values indicated in Table 2, not considered, because a lack of fwhm values in the alcoholic solvents makes a trend too uncertain to discuss. Vibrations #B, #D−H, and and #L−M showed no significant change in fwhm values and will not be considered further. Four vibrations, #C−F, show consistent decreases in I_N when going from alcoholic solvents to non-alcoholic solvents. I_N of vibration #C decreases (average for alcoholic solvents to average of nonalcoholic solvents) from 0.57 to 0.46, vibration #D from 0.67 to 0.60, vibration #E from 0.57 to 0.46, and vibration #F from 1.13 to 1.03. Vibrations #A−B and #G−K show no change of I_N, either because of solvent band interference or the intensity varies so that no clear trend can be observed.

In Figure 2 the doublet at ~1600 cm^{-1} is displayed. The spectra (thick lines) display two components (thinner lines) corresponding to vibrations #L and #M. Vibration #L shows characteristic shifts in band intensities. For VA in EtOH, MeOH, and PrOH the intensity ratio, I_N, of this vibration is ~0.7, whereas in Ace, THF, and Diox a value of 0.43 is obtained.

Considering the changes in band center wavenumbers, vibration #A is the only vibration that shows a clear decrease in ω_C when changing the solvents. From alcohol to non-alcohol solvents, the average change is from 365 to 358 cm^{-1}. With a spectral

Table 1. List of VA Center Wavenumbers (ω_C), Normalized Intensities (I_N), and FWHM[a]

	ω_C (cm^{-1})						I_N						fwhm (cm^{-1})					
Vib	MeOH	EtOH	PrOH	Ace	Diox	THF	MeOH	EtOH	PrOH	Ace	Diox	THF	MeOH	EtOH	PrOH	Ace	Diox	THF
A	363	367		358	359	358	0.24	0.17		0.23	0.22	0.20	26.1	24.8		22.7	24.1	24.4
B	403	402	403	399	400	401	0.71	0.69	0.62	0.69	0.60	0.53	16.9	16.1	14.8	17.8	15.6	16.9
C	565	563	565	561	562	562	0.54	0.59	0.59	0.49	0.48	0.41	18.1	23.4	22.6	18.0	14.9	17.8
D	720	719	718	718	718	719	0.65	0.66	0.68	0.62	0.61	0.57	12.4	12.9	11.2	12.9	12.0	12.5
E	739	739	738	737	737	737	0.58	0.60	0.53	0.47	0.49	0.43	13.0	12.1	12.7	15.1	12.3	11.9
F	796	796	796		795	796	1.16	1.12	1.11		1.07	0.98	11.9	12.5	11.8		11.9	12.4
G	921	920	920	918	918	921	0.40	0.39	0.28	0.35	0.29	0.49	12.6	12.7	9.6	14.8	12.9	11.1
H	934	934		932	931	934	0.14	0.19		0.16	0.14	0.10	12.1	12.4		12.8	15.1	9.1
I		1036		1035	1035	1034		0.27		0.29	0.20	0.42		12.9		12.5	13.7	19.8
J	1189	1189	1189	1185	1186	1186	0.36	0.34	0.33	0.32	0.31	0.32	13.7	12.7	9.6	17.2	14.2	13.9
K	1278			1277	1276	1278	0.49			0.60	0.55	0.59	21.3			20.8	16.8	21.7
L	1604	1603	1604	1602	1602	1602	0.68	0.70	0.70	0.42	0.44	0.41	16.6	14.7	15.4	14.0	15.0	15.7
M	1615	1614	1614	1614	1613	1614	1.00	1.00	1.00	1.00	1.00	1.00	13.5	12.4	12.7	11.6	11.9	12.8

[a] Prior to Lorentz fitting, the intensities have been normalized with respect to vibration # M at approximately 1614 cm^{-1}. Only bands with an average intensity ratio >0.14 are displayed in the table. Vacancies in the table are due to the fact that interference by solvent bands prohibited reliable data.

Table 2. Comparison of Average (Ave), Standard Deviation (STD), and Difference (Dif) of the VA ω_C, I_N, and FWHM in the Alcohol and Non-Alcohol Solvents[a]

	ω_C (cm^{-1})					I_N					fwhm (cm^{-1})				
Vib	Ave. Alc	STD (cm^{-1})	ave. nonalc	STD (cm^{-1})	Dif	ave. Alc	STD (%)	ave. nonalc	STD (%)	Dif /%	ave. alc	STD (cm^{-1})	ave. nonalc	STD (cm^{-1})	Dif
A	365	2.8	358	0.6	6.7	0.205	10.9	0.217	1.5	−1.2	25.5	0.9	23.7	0.9	1.7
B	403	0.6	400	1.0	2.7	0.673	4.7	0.607	8.0	6.7	15.9	1.1	16.8	1.1	−0.8
C	564	1.2	562	0.6	2.7	0.573	2.9	0.460	4.4	11.3	21.4	2.9	16.9	1.7	4.5
D	719	1.0	718	0.6	0.7	0.663	1.5	0.600	2.7	6.3	12.2	0.9	12.5	0.5	−0.3
E	739	0.6	737	0.0	1.7	0.570	3.6	0.463	3.1	10.7	12.6	0.5	13.1	1.7	−0.5
F	796	0.0	796	0.7	0.5	1.130	2.7	1.025	6.4	10.5	12.1	0.4	12.2	0.4	−0.1
G	920	0.6	919	1.7	1.3	0.357	6.7	0.377	10.3	−2.0	11.6	1.8	12.9	1.9	−1.3
H	934	0.0	932	1.5	1.7	0.165	8.5	0.133	3.1	3.2	12.3	0.2	12.3	3.0	−0.1
I	1036	nv	1035	0.6	1.3	0.270	nv	0.303	11.1	−3.3	12.9	nv	15.3	3.9	−2.4
J	1189	0.0	1186	0.6	3.3	0.343	0.0	0.317	0.6	2.7	12.0	4.8	15.1	1.8	−3.1
K	1278	nv	1277	1.0	1.0	0.490	nv	0.580	2.7	−9.0	21.3	nv	19.8	2.6	1.5
L	1604	0.6	1602	0.0	1.7	0.693	1.2	0.423	1.5	27.0	15.6	1.0	14.9	0.9	0.7
M	1614	0.6	1614	0.6	0.7	1.000		1.000		0.0	12.9	0.6	12.1	0.6	0.8

[a] The STDs for the intensities are shown in percentage of the normalized band at 1614 cm^{-1}. nv: no value.

resolution of 4 cm^{-1}, band positional shifts >4 cm^{-1} are considered significant, whereas smaller shifts are considered too uncertain, i.e., less significant. Only shifts less than 4 cm^{-1} are observed for all other vibrations #B−M. Therefore, no clear ω_C trends are found for these vibrations, neither as a function of dielectrical constants of the solvents nor dependent on the solvents ability to function as hydrogen bond donor/acceptor.

Predicted Raman Spectra. Spectra of VA are predicted in ethanol, methanol, acetone, and tetrahydrofuran. VA has twelve different conformers which are combinations of the conformers of the substituents on the aromatic ring, where the individual phenyl−OH and methoxy group conformations combine to a total of four.[35] These conformers were also investigated for 2-methoxyphenol by Agache and Popa[36] with the result that the cisoid structure is stabilized by intramolecular hydrogen bonding between the phenyl−OH and the methoxy group which makes it by far the most stable. In the present work this is therefore the only conformation considered for VA with respect to these groups. This reduces the number of conformations to those which the benzyl hydroxy group can adopt. Three local minimum energy conformations were identified at the B3LYP/6-31+G(d) (vacuum) level of theory by a systematic scanning of the energy as function of the two relevant dihedral angles; see Figure 3. These conformers were verified by a subsequent harmonic frequency calculation which produced no negative frequencies (results not shown).

The Gibbs free energy of each conformer is calculated by the PCM/B3LYP/6-31+G(d) model, and their population probabilities are given by

$$p_i = Ae^{-G_i/(k_B T)}$$

where k_B is the Boltzmann factor, T is the temperature, and A is determined by the normalization condition

$$\sum p_i = 1$$

The energies and probabilities are listed in Table 3.

After mode by mode matching between conformers A−C the weighted predicted wavenumbers and Raman intensities were calculated using the distribution percentages given in Table 3. The calculated data are given in Table 4. Only modes corresponding to the experimental interval 1800−300 cm^{-1} have been included.

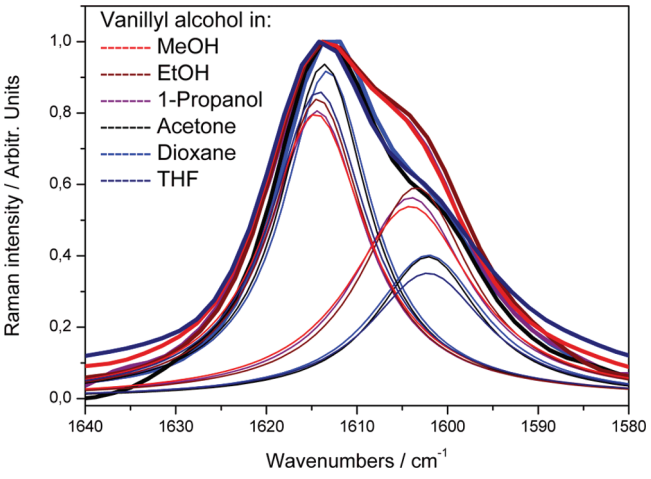

Figure 2. Raman spectra in the 1640−1580 cm^{-1} interval of vanillyl alcohol dissolved in six different solvents. The thicker lines are the baseline corrected spectra, whereas thinner lines are their resolution into two Lorentzians.

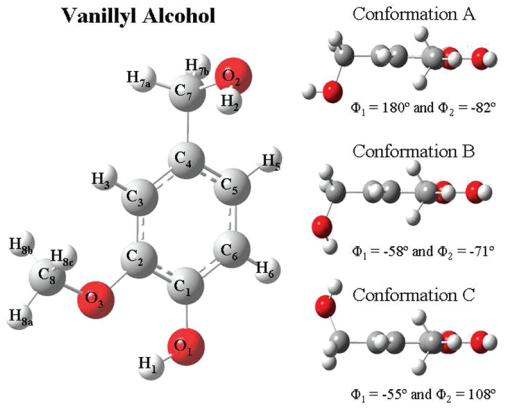

Figure 3. Three dominant conformations of vanillyl alcohol, defined by two dihedral angles: $\Phi_1(C_4-C_7-O_2-H_2)$ and $\Phi_2(C_3-C_4-C_7-O_2)$.

Comparison of Predicted and Observed Data. Harmonic wavenumbers predicted by electronic structure calculations are usually higher than the experimental fundamental wavenumbers due to a combination of improper description of electron correlation effects, basis set deficiencies and (mainly) neglect of anharmonicities. The errors in the calculations are largely systematic and can be corrected by empirical scaling factors. Several studies on determining scaling factors for achieving fundamental vibrational wavenumbers from predicted harmonic wavenumbers have been performed, and these factors depend on the calculational method and basis set.[37−44] Various methods have been devised to obtain scaling factors, e.g., by linear least-squares fitting procedure,[43−45] local scaling factors[46−49] or using the effective scaling frequency approach (ESFF).[47−51] Using a single scaling factor is the simplest way to correct for anharmonicities, and a recommended single factor using B3LYP with the basis set 6-31 +G(d) is $f = 0.9636$.[40] Though, in the present work two different wavenumber scaling constants were determined. The procedure is described below.

To facilitate the comparison between calculated and observed data, the Raman spectra have been divided into two intervals: 1700−950 and 950−300 cm^{-1}. For each interval a single band has been chosen to be the normalization band. In the interval 1700−950 cm^{-1}, the predicted wavenumbers are scaled using the observed band at 1614 cm^{-1} (peak #M). In the interval 950−300 cm^{-1}, the predicted wavenumbers are scaled using the band at 796 cm^{-1} (#F). The factors used to scale the wavenumbers are therefore (1614 cm^{-1}/1651 cm^{-1} =) 0.9782 and (796 cm^{-1}/ 806 cm^{-1} =) 0.9888 for the high and low wavenumber interval, respectively. Both wavenumber scale factors (0.9782 and 0.9888) are higher numbers than the recommended frequency scale factor (0.9636), resulting in a smaller scaling effect than usual. This is mainly due to neglect of wavenumbers higher than 1700 cm^{-1} in this study. These higher wavenumber vibrations, i.e., νOH and νCH modes, have relatively large anharmonicities. Another inappropriate feature of published scaling factors is the fact that they are based on a general set of molecules many of which are structurally very different from the C, O and H based lignin structures. In the present work the two scaling factors are thus more appropriate in this sense. Their precise values are, however, of little practical consequence as a ±0.01 error of their values amounts to a ∼3−17 cm^{-1} position error, which is likely not larger than the inherent errors of the method/basis set chosen.

In order to compare the predicted Raman activities to the strengths of observed bands a normalization procedure was employed for both the strengths of observed bands as well as for the predicted activity values and the simulated bands derived from these. They were in each of the two wavenumber intervals all normalized by the activity value or peak height of the most dominant Raman band, i.e. the #M/#47 and

Table 3. Gibbs Free Energies and Probabilities of the Distribution of the Three Conformers in THF, Acetone, EtOH, and MeOH Calculated Using B3LYP 6-31+G(d) Basis Set at Room Temperature

	Gibbs free energies (hartree)			conformation distribution (%)		
solvent\conformation	A	B	C	A	B	C
THF	−536.422301	−536.424317	−536.422969	8.7	73.6	17.7
Ace	−536.426165	−536.428935	−536.427181	4.4	82.7	12.9
EtOH	−536.426806	−536.428766	−536.427695	8.7	69.1	22.2
MeOH	−536.427616	−536.428058	−536.428460	19.8	31.7	48.5

Table 4. Predicted Data for VA in the Four Solvents THF, Ace, EtOH, and MeOH Found As a Weighted Average of the Predicted Data of the Three Conformations[a]

	PCM B3LYP 6-31+G(d) predictions of vanillyl alcohol							
	wavenumbers (cm^{-1})				Raman scattering activities (A^4/AMU)[b]			
mode	MeOH	EtOH	Ace	THF	MeOH	EtOH	Ace	THF
9	**307**	**310**	**314**	**323**	**0.01**	**0.01**	**0.01**	**0.02**
10	**321**	**325**	**327**	**348**	**0.01**	**0.02**	**0.02**	**0.02**
11	**365**	**368**	**368**	**368**	**0.03**	**0.02**	**0.02**	**0.02**
12	**402**	**404**	**405**	**404**	**0.08**	**0.07**	**0.08**	**0.08**
13	464	462	461	461	0.01	0.01	0.01	0.01
14	501	503	505	505	0.01	0.01	0.01	0.01
15	**553**	**552**	**552**	**552**	**0.02**	**0.02**	**0.02**	**0.02**
16	**561**	**561**	**561**	**560**	**0.07**	**0.07**	**0.07**	**0.08**
17	646	645	644	644	0.03	0.03	0.03	0.03
18	**717**	**717**	**717**	**716**	**0.05**	**0.05**	**0.05**	**0.05**
19	**743**	**742**	**742**	**742**	**0.09**	**0.10**	**0.10**	**0.11**
20	**804**	**805**	**805**	**806**	**0.24**	**0.24**	**0.24**	**0.26**
21	833	833	833	834	0.04	0.04	0.05	0.04
22	872	872	872	872	0.02	0.02	0.02	0.02
23	**931**	**930**	**929**	**930**	**0.16**	**0.15**	**0.14**	**0.15**
24	**947**	**947**	**946**	**947**	**0.01**	**0.01**	**0.01**	**0.01**
25	982	987	988	990	0.07	0.04	0.03	0.04
26	**1012**	**1010**	**1009**	**1013**	**0.18**	**0.22**	**0.23**	**0.23**
27	1053	1053	1053	1055	0.04	0.04	0.04	0.04
28	1139	1139	1139	1140	0.04	0.05	0.06	0.05
29	1176	1178	1177	1178	0.03	0.03	0.03	0.03
30	1179	1178	1178	1179	0.02	0.02	0.01	0.04
31	**1187**	**1186**	**1185**	**1189**	**0.43**	**0.48**	**0.50**	**0.48**
32	1202	1201	1201	1202	0.07	0.06	0.06	0.07
33	1224	1223	1222	1224	0.04	0.04	0.05	0.05
34	1254	1255	1255	1256	0.03	0.02	0.02	0.02
35	**1295**	**1298**	**1299**	**1299**	**0.50**	**0.56**	**0.58**	**0.54**
36	1321	1322	1323	1322	0.16	0.09	0.07	0.09
37	1358	1362	1363	1361	0.05	0.05	0.05	0.05
38	1395	1397	1397	1400	0.18	0.19	0.20	0.20
39	1422	1419	1417	1420	0.25	0.31	0.33	0.35
40	1463	1463	1463	1464	0.04	0.05	0.05	0.05
41	1495	1495	1495	1496	0.07	0.07	0.08	0.08
42	1507	1507	1507	1508	0.14	0.15	0.16	0.17
43	1516	1516	1516	1518	0.12	0.14	0.14	0.14
44	1519	1517	1518	1519	0.08	0.08	0.08	0.10
45	1548	1548	1547	1549	0.03	0.04	0.04	0.04
46	**1642**	**1642**	**1642**	**1644**	**0.38**	**0.41**	**0.42**	**0.47**
47	**1649**	**1649**	**1649**	**1651**	**1.00**	**1.00**	**1.00**	**1.00**

[a] The wavenumbers are unscaled values. The modes and corresponding values given in bold correspond to the experimentally observed bands (see section comparing predicted and observed data). [b] The Raman scattering activities are expressed in units of that of mode #47, the activity of which is predicted as (in units of $Å^4$/amu) 133.2 in THF, 159.4 in Ace, 165.4 in EtOH, and 176.8 in MeOH.

#F/#20 vibrations located in the intervals 1700−950 and 950−300 cm^{-1}, respectively.

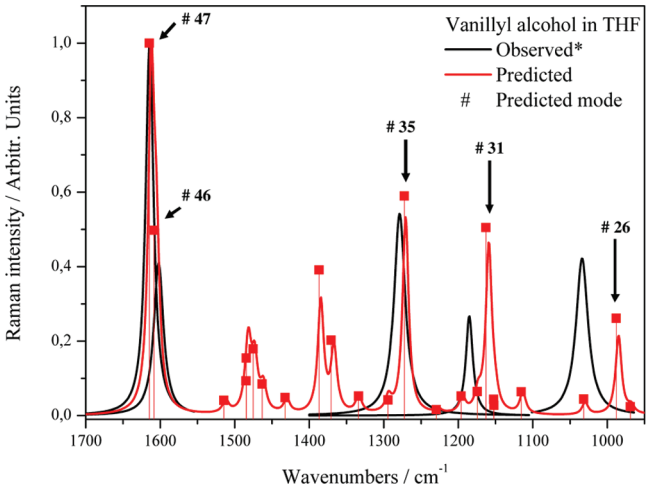

Figure 4. Raman spectrum of VA in THF in the interval 1700−950 cm^{-1}. The black curves are the Lorentzians fitted to the experimentally observed Raman bands, and the red curve is the predicted Raman spectrum based on the predicted positions/intensities (red squares). The numbers of predicted normal modes are shown. All data have been normalized and scaled after the band at 1614 cm^{-1}. The original data for these modes can be found in Table 4.

In the following the observed Raman bands of solvated VA are exemplified by the spectrum obtained in THF (shown in terms of its Lorentz fit components), and selected wavenumber intervals of this spectrum are depicted together with the corresponding PCM/B3LYP predicted spectrum of VA dissolved in THF. As is demonstrated by this solvent, the PCM/B3LYP procedure reproduces the experimental Raman spectrum fairly well except for some discrepancies which will be examined more closely.

1700−950 cm^{-1} Interval. In Figure 4 the Lorentz fit of VA bands in THF and the predicted spectrum is displayed for the interval 1700−950 cm^{-1}. The spectrum is in this region normalized after the vibration at 1614 cm^{-1}.

In the 1700−950 cm^{-1} interval five bands were found in the experimental spectra (#J-M) and 23 normal modes were predicted (#25−47).

The bands #K, #L, and #M at 1278, 1604, and 1615 cm^{-1}, respectively, correspond well with the predicted modes #35, #46, and #47. The band #J at 1189 cm^{-1} is tentatively assigned the predicted mode #31. Although the wavenumbers of other predicted modes compare more favorably their predicted intensities do not. The observed band #I at 1035 cm^{-1} appears to be even more difficult to assign. The relatively large intensity of the predicted mode #26 at 991 cm^{-1} suggests that this mode corresponds to the #I band and in that case has a much too low predicted position. The experimental spectrum (not shown) reveals, after subtracting two THF bands at 1030 cm^{-1} and 1071 cm^{-1}, that there is a weak band at 1059 cm^{-1} and a shoulder on the #I band at 1012 cm^{-1}. We suggest these bands to correspond with the predicted bands #27 at 1032 cm^{-1} and #25 at 968 cm^{-1}, respectively, and that the #I band corresponds to #26 despite the low predicted wavenumber.

950−300 cm^{-1} Interval. In Figure 5 the interval 950−300 cm^{-1} is displayed. The correspondence between observed and predicted bands is more convincing in this interval, where eight bands are found in the experimental spectra (#A−I) and 16 normal modes are predicted (#9−24).

dx.doi.org/10.1021/jp203910h |J. Phys. Chem. B 2011, 115, 11470–11480

The predicted modes #24, #23, #20, and #19 are all in good agreement with the experimental modes at 934, 921, 796, and 739 cm^{-1}, respectively. #18 is predicted at lower wavenumber and significantly less intensity compared to the experimentally observed band at 720 cm^{-1}. The predicted modes #16 and #15 can be assigned to the broad band #C observed at 562 cm^{-1}, thereby revealing this band as a two-component band. The predicted mode #12 is assigned to the observed band #B at 401 cm^{-1}, and one or several of the predicted modes #9−11 appear to be responsible for the broad band #A observed at 358 cm^{-1}.

The predicted mode #22 at 860 cm^{-1} can, although not shown in Figure 5, be found in the experimental spectrum. However, the band is a weak shoulder on an intense THF band and cannot be reliably included in the observations. For the same reason an observed band corresponding to #21 is not included.

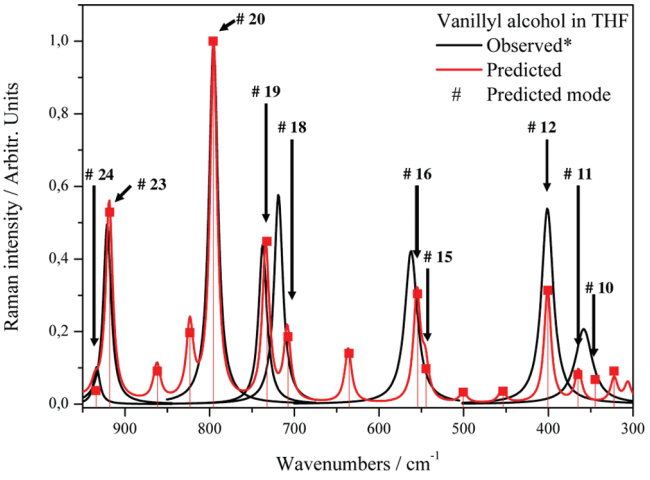

Figure 5. Raman spectrum of VA in THF in the interval 950−300 cm^{-1}. The original data for these modes can be found in Table 4.

The discrepancy between #18 and the observed band at 720 cm^{-1} can have different causes. It may be explained by the inadequacy of the calculational method, where, e.g., the basis set chosen is not comprehensive enough for reliable Raman intensity calculations, or it may not reflect that the experimental band is enhanced because of Fermi resonance with the intense close lying band at 741 cm^{-1} (#19). The predicted mode #17 appears in the experimental spectrum of VA in THF as a very weak band, but like mode #22, it is disregarded due to overlap with THF solvent bands.

Vibrational Description. In Table 5, the predicted modes are described together with tentative assignments to the observed (Lorentzian) band components.

DISCUSSION

A comparison of the predicted vibrations for VA in the four different solvents (Table 4) shows that their positional differences as a function of solvent are small; the standard deviation (of the four values) STD averaged over #11−47 equals STD = 1.7 cm^{-1}. For vibration #9 its predicted position in THF is higher, i.e., 323 cm^{-1}, than in Ace, EtOH, and MeOH, i.e., 307−314 cm^{-1}. For vibration #10, this is even more pronounced with 348 cm^{-1} in THF and 321−327 cm^{-1} in Ace, EtOH, and MeOH. These differences could be caused by a dependency on the dielectrical constant. The predicted positions for the vibrational modes in Ace are more similar to those in EtOH and MeOH. Therefore within the PCM approach the predictions do not support the hypothesis that the observed shifts as function of solvents are a function of solvent ability to act as a hydrogen and/or electron donor. The calculations do not predict the experimentally observed changes in intensities. PCM is a mean field model and fails to explain changes caused by the specific localized hydrogen bonding ability of the solute. An alternative could be using a supramolecular approach combined with PCM where

Table 5. List of the Predicted Vibrations for VA in THF Assigned to the Experimentally Observed Bands with Intensities >0.14 after Normalization[a]

predicted mode	experi-mental mode	predicted ν (cm^{-1})	predicted and scaled (cm^{-1})	exp. ω_C (cm^{-1})	vibrational description	mode type
#47	M	1651	1615	1614	$\nu_s(C_2-C_3;C_5-C_6)$, $\nu_s(C_3-C_4;C_1-C_6)$, $\delta(C_1-O_1-H_1)$	Ip
#46	L	1644	1608	1602	$\nu_s(C_1-C_2;C_4-C_5)$, $\delta(C_1-O_1-H_1)$	Ip
#35	K	1301	1273	1278	$\nu_s(C_1-O_1;C_2-O_3;C_4-O_7)$, Rd	Ip
#31	J	1189	1163	1186	$\delta(C_1-O_1-H_1)$, Rd (ip)	P
#26	I	1010	988	1034	$\nu(C_7-O_2)$, $\gamma(C_{ar}-C_4-C_7)$	Oop
#24	H	946	935	934	$\gamma_a(C_5-H_5; C_6-H_6)$	Oop
#23	G	929	919	921	$\gamma(C_6-H_6)$, $\gamma_a(C_4-C_7-H_{7a};C_4-C_7-H_{7b})$, $\delta(C_4-C_5-C_6)$, $\delta(C_7-O_2-H_2)$	Oop
#20	F	806	797	796	$\delta(C_3-C_4-C_5)$, $\gamma_s(C_3-H_3; C_5-H_5; C_6-H_6)$, $\nu(C_1-O_1)$	Oop
#19	E	741	733	737	$\gamma(C_{ar}-C_4-C_7)$, Rd (oop)	Oop
#18	D	716	708	719	$\gamma(C_{ar}-C_1-O_1)$, Rd (oop)	Oop
#16	C	561	555	562	$\gamma_a(C_1-O_1-H_1; C_2-C_3-C_4)$	Ip
#15	C	551	545	562	$\delta_s(C_2-C_1-O_1; C_3-C_2-O_3; C_7-C_4-C_5)$, $\delta(C_8-O_3-C_2)$	Ip
#12	B	406	401	401	$\gamma_a(C_{ar}-C_4-C_7; C_{ar}-C_1-O_1)$, Rd (oop), $\gamma(O_2-H_2)$	Oop
#11	A	369	365	358	$\gamma(O_2-H_2)$, $\delta_s(C_8-O_3-C_2; C_7-C_4-C_5)$	Oop
#10	A	349	345	358	$\tau(O_2-H_2)$, τ (O_1-H_1),	Oop
#9	A	326	322	358	$\gamma(O_2-H_2)$, $\delta_s(C_8-O_3-C_2; C_2-C_1-O_1)$	Oop

[a] The assigned predicted mode, the assigned observed mode, the predicted wavenumber, the predicted and scaled wavenumber, the observed wavenumber, and the vibrational description. In the vibrational description, the mode types are in plane, ip, and out of plane, oop compared to the aromatic plane, ν: stretch, γ: out of plane bend, δ: in plane bend, Rd: ring deformation, τ: torsion, s: symmetric and a: asymmetric.

dx.doi.org/10.1021/jp203910h |J. Phys. Chem. B 2011, 115, 11470–11480

some of the solvent molecules are explicitly modeled and contained within the cavity of the solute and thereby described at an explicit quantum mechanical level.[52−54] However, the mean field PCM is a computational cheap method to describe the vibrations that are found experimentally to change as a function of hydrogen bonding.

Prior to these findings, the dependence of Raman band shape and position was investigated by increasing the concentration of models in solution to a maximum with regard to the solubility. The results suggested that the band positions did not shift as a function of concentration. The intensities increased as function of concentration as compared to the solvents; however, the relative intensities of model bands were not found to change. The lack of positional and relative intensity shifts as function of concentration were used as a validation that the model of weak solute−solute interactions, e.g., no complex formation. The models were all considered to be monomers surrounded by solvent molecules. The temperature dependence was not a subject of investigations. The experiments were carried out at room temperature. This study demonstrates how predictions can help assign Raman vibrational band, which can be seen to change experimentally as a function of solvents. However a change of Raman spectra in different solvents as function of temperature were not the focus, and have not been investigated.

A previous study on predicting phenol vibrations has shown that B3LYP harmonic wavenumber calculations show an overall basis set dependency on the type of normal mode.[55] In plane (ip) mode wavenumbers require a smaller size basis set than out of plane (oop) modes, which are very demanding in terms of basis set flexibility.

Experimentally it was found that the peak shape of the doublet at about 1600 cm^{-1} showed dependency on whether the solvent could act as hydrogen donor. The predictions of the relative Raman activities for this doublet $I_{\#46}/I_{\#47}$ are: 0.47 and 0.42 in THF and Ace, whereas they are 0.41 and 0.38 in EtOH and MeOH. These predictions show a decrease in ratio when going from a solvent unable to act as a hydrogen (bond) donor to a solvent capable of donating hydrogen (bonds). These findings contradict the observations, where $I_{\#46}/I_{\#47}$ = 0.41 and 0.42 in THF and Ace but 0.70 and 0.68 in EtOH and MeOH. Although the predicted activity ratios are not in accordance with the observed the fact that this ratio is solvent dependent is suggested by the nature of the two predicted vibrations of this doublet. The two modes are two different aromatic stretching vibrations with a contribution of the phenolic OH ip bend (see Table 5 for precise atoms involved in the vibrations). This bending vibration is predicted as slightly more pronounced in mode #46, which could explain why there is a relative difference of the intensity change of the two modes as a function of hydrogen bonding ability of the solvent.

The predicted mode #31 is primarily a C_{ar}−O−H ip bending with a contribution from ring deformation. Vibrations involving the O−H groups, which can function both as donors and acceptors, are expected to be more prone to be affected by hydrogen bonding. Therefore, the OH ip bending contribution is likely responsible why #31, observed at 1189 cm^{-1} for VA in MeOH, EtOH, and PrOH shifts to a slightly lower wavenumber, 1186 cm^{-1}, for VA in Diox and THF and 1185 cm^{-1} in Ace, while the intensity of this band is only slightly decreased from ∼0.34 in MeOH, EtOH, and PrOH to ∼0.32 in Ace, Diox, and THF. It may also explain why a change in experimentally obtained fwhm is seen for #J (#31), where the fwhm increases from ∼12 cm^{-1} in alcoholic solvents to ∼15 cm^{-1} in non-alcoholic solvents.

The modes #25−27 show larger discrepancies from the observed bands than other predicted VA bands. The intense band at 1035 cm^{-1} is predicted at 991 cm^{-1} (#26), the weak shoulder found at 1012 cm^{-1} is predicted at 968 cm^{-1} (#25), and the weak band at 1059 cm^{-1} is predicted at 1032 cm^{-1} (#27). Discrepancies between observed and predicted wavenumbers could be due to the fact that the scaling factor (0.9782) is in this interval determined by the band at ∼1600 cm^{-1}, whereas these bands lies at the borderline of the other interval, ω_C < 950 cm^{-1}, with a scale factor of 0.9888. This causes the predicted bands to be scaled to a too low value. Another explanation is that #25 and #26 are out of plan vibrations, which is known to be more problematic to predict correctly.[55]

The VA oop modes #9, #10, and #11 are all assigned to the experimentally observed band at 363 cm^{-1}. Increasing the size of the basis set could offer an accurate assignment of this band to the correct oop mode. The PCM predictions showed that #10 shifts position as a function of solvent. The absolute predicted difference between THF and Ace, EtOH and MeOH were ∼27 cm^{-1}. However, the predicted wavenumber for this mode is highest in THF, which the experimental data contradicts. The predicted mode #10 is a combination of C_{ar}−O-H oop torsion and $C_{aliphatic}$−O−H oop torsion. The experimentally observed band at 363 cm^{-1} (MeOH) and 367 cm^{-1} (EtOH) shifts to a lower wavenumber for the acceptor solvents, 358 cm^{-1} (Ace), 359 cm^{-1} (Diox) and 358 cm^{-1} (THF). From the comparison with predicted data it is difficult only to assign this observed band to the predicted mode #10 as modes #9 and 11 are predicted in close proximity. Mode #9 is dominated by C_{al}−O−H oop bending, with a small contribution of $C_{aliphatic}$−O−C_{ar} and C_{ar}−C_{ar}−O ip bending vibrations. Mode #11 consists of a combination of C_{al}−O−H oop bending, C_{al}−O−C_{ar} and C_{ar}−C_{ar}−C_{al} ip bending. Mode #9, #10 and #11 all involve C_{al}−O-H bending vibrations, which could explain the wavenumber shift as function of solvent. As opposed to the doublet at ∼1600 cm^{-1}, the experimental observed band at 360 cm^{-1} shows no clear trends of intensity dependence on the solvents.

Vanillyl Alcohol As a Lignin Model Monomer. The results above have positive implications for the attempts to examine how substitution influences lignin (model) Raman spectra.

Lignin is formed from three phenolic precursors containing none, one, or two OMe groups, i.e., H, G, and S units, respectively. We have previously shown that for the lignin model monomers 4-methylphenol (H), 2-methoxy-4-methylphenol (G), and 2,6-dimethoxy-4-methylphenol (S), two more or less overlapping bands were observed in the Raman spectra in the interval between 1650 and 1550 cm^{-1} and that two different aromatic ring deformations are responsible for this band,[35] which is thus a two-component band for all three lignin model monomers. The PCM/B3LYP/6-31+G(d) calculated difference in band positions for these two components was predicted as 24 cm^{-1} (H), 5 cm^{-1} (G), and 14 cm^{-1} (S), and the corresponding Raman activity ratios as (high wavenumber/low wavenumber) 4:1 (H), 5:1 (G), and 1:9 (S) for the (model) CCl_4 solvent. These two modes are described as two different C_{ar}−C_{ar} stretches; one compressing the benzene ring in the direction aligned with the hydroxy C−O(H) bond (direction 1) and one compressing the benzene ring along two other C_{ar}-C_{ar} (direction 2, see Table 5 and Figure 3). These bands show a predicted opposite positional shift as a function of adding

methoxy groups, $C_{ar}-C_{ar}$, (dir 1) 1606 cm^{-1} (H) → 1599 cm^{-1} (G) → 1586 cm^{-1} (S) and for the $C_{ar}-C_{ar}$ (dir. 2), 1582 cm^{-1} (H) → 1594 cm^{-1} (G) → 1600 cm^{-1} (S). Also, the intensity difference increases as a function of adding methoxy groups.

This study shows the range of solvent induced wavenumber shift for VA to be around 2 cm^{-1} for the predicted mode #46 and no change for the predicted mode #47. Therefore, the expected solvent or environment induced shifts are significantly less than the shift between the three types of lignin model compounds.

Further, this study shows that the experimental intensity ratio $I_{\#46}/I_{\#47}$ changes from ∼0.7 in MeOH, EtOH, and PrOH to ∼0.43 in Ace, Diox, and THF.

VA compares best with the G-model monomer, since both contain a single methoxy group. When comparing the intensity ratio of the doublet at about 1600 cm^{-1} of the G unit and VA some discrepancies are found. Predicted ratios change from 0.2 for the G-model[35] (in CCl_4) to 0.37 for VA in CCl_4 (data not shown), 0.47 (VA in THF), 0.42 (VA in Ace), to 0.41 (VA in EtOH) to 0.38 (VA in MeOH). The predicted intensity ratio of mode #46 relative to #47 shows an opposite tendency as function of the solvents compared to the experiments. The intensity ratio is predicted to increase from ∼0.40 (alcohol solvent) to ∼0.45 (nonalcohol solvent), whereas experimentally it decreases from ∼0.70 (alcohol solvent) to ∼0.42 (nonalcohol solvent). This behavior is therefore not even qualitatively explained by the predicted data of the different solvents. The DFT/PCM predicted Raman intensities should therefore be considered more qualitatively than quantitatively, and in relation to the more subtle solvent (shift) effects they do not compare with experiments. The experimental ratios for the H, G, and S models in CCl_4 respectively are: 0.63, 0.49, and 0.55. Thus from the results of VA it can be expected that solvent effects on this ratio are significant compared to the substitution (H, G, or S) effect.

CONCLUSIONS

Experimental NIR FT Raman spectra have been obtained of vanillyl alcohol in the solvents MeOH, EtOH, PrOH, Ace, Diox and THF. The interval 1700−300 cm^{-1} was investigated for the change of band characteristics in terms of fwhm, wavenumber positions and intensities as a function of solvent ability to act as hydrogen and/or electron donor. Thirteen bands were observed with intensity ratio >0.14 (relative to the 1614 cm^{-1} band) in the interval 1700−300 cm^{-1}. Three bands, #A, #C, and #J, were found to change fwhm as a function of solvent type. A change in intensity was found to a minor degree for the bands #C−F, but for band #L, positioned at 1602 cm^{-1}, the intensity decreased from 0.70 in the alcoholic solvents (hydrogen and electron donors) to 0.42 in the non-alcoholic solvents (electron donors). A relatively large shift in wavenumbers were observed for the bands around 363 cm^{-1} (shift ∼7 cm^{-1}), and a small shift for the bands at 1189 cm^{-1} (shift ∼3 cm^{-1}).

The predicted data was then used to tentatively assign the modes giving rise to the observed bands in the experimental spectra. The doublet around 1600 cm^{-1} is assigned two different aromatic C═C stretching vibrations, both with a contribution of $C_{ar}-O-H$ ip bend. The band at 1602 cm^{-1} contains more contribution from this ip bend than the band at 1614 cm^{-1}, which is a likely reason for the solvent dependency of its intensity ratio, i.e., band shape of the 1600 cm^{-1} doublet band. Two bands at 1189 and 363 cm^{-1} were identified with a significant change of position as a function of solvent. Their corresponding vibrations both contain significant $C_{ar/al}-O-H$ bend, i.e., in plane vibration for the 1189 cm^{-1} band and out of plane for the 363 cm^{-1} band. The band at 1189 cm^{-1} also displayed the largest shift in fwhm values, which changed with ∼4 cm^{-1}.

The comparison of experimental and predicted Raman bands of VA in different solvent environments shows that the PCM is not even adequate for a qualitative prediction of the solvent dependency of Raman band properties. It appears that the PCM performs reasonably well only in the sense that it does predict whether a vibration can be expected solvent sensitive or not. We ascribe this to the fact that this depends on the presence of certain vibrational types for a given normal mode. Thus normal modes with contributions from OH vibrations (torsional, bending, etc.) are sensitive to the hydrogen bonding ability of the solvent or environment since OH groups participate in such interactions. The PCM predicts solvent dependency of such modes since their vibrations involve (relatively large) changes of charges and charge distributions, which this model (by its very construction) is sensitive toward. The PCM gives correct semiquantitative predictions for simple compounds in regard to, e.g., simple carbonyl vibrations[56−60] but the present results show that for lignin model compounds such as VA qualitative correct predictions probably require use of explicit solvent models. Thus, apart from providing a qualitative indication of solvent dependency (but none in relation to its direction) of lignin model vibrational modes, the PCM is not of much use, and most relevant information for assignment of spectra can be obtained from standard ("vacuum") DFT.

Therefore PCM using the B3LYP/6-31+G(d) basis set is thus only recommended to predict and assign vibrations that leads to experimentally observed band but is not suited for more subtle predictions of band positional or intensity shifts caused by solute−solvent interactions. For a more accurate prediction of Raman activity dependence on choice of solvent an approach can be to use a better XC functional such as CAM-B3PW91 or ab initio methods, e.g., CAS-PT2/PT3, and treating the solvent using explicit solvent model for first solvation/hydration shell as has been shown for example for L-alanine.[27,29−32] This may allow for a more precise description of solvent effects on the lignin model compound and will be a subject for future work.

The doublet around 1600 cm^{-1} has previously shown potential to differentiate between the three lignin H, G, and S units.[11,35] The lack of significant wavenumber changes of the doublet components as a function of solvent found in this study of VA indicates that a wavenumber change seen in the Raman spectra of different lignin model compounds are largely explained by the effect of adding methoxy groups, and will not be affected to a similar degree by the surroundings in different solvents. However, the ratio of the intensities of the doublet components was observed to be solvent dependent.

The present work has thus shed light on the complex nature of the well-known 1600 cm^{-1} Raman band of lignin. This band is a superposition of H, G, and S unit bands each consisting of two components characteristic of the aromaticity of these units. The present work has shown that for phenolic units the wavenumber position of these components are mainly indicative of the methoxyl substitution, i.e., distinguishes H, G, and S units, whereas their relative intensities also depend on solvent or environment even though the (H,G) → S substitution still dominates the intensity change. The existence of environment dependency of intensity appears to characterize all vibrational modes, which have considerable contributions from OH groups.

Thus the relative Raman intensities of such modes, e.g., the shape of the 1600 cm^{-1} doublet, can in principle be used to give an indication of the environment of lignin. In practice this is complicated by the high degree of spectral overlap of bands from H, G, and S units, e.g., as both observed and predicted for the 1600 cm^{-1} doublet.

AUTHOR INFORMATION

Corresponding Author

*E-mail: sbar@life.ku.dk. Phone: +45 35331686. Fax: +45 35331508.

ACKNOWLEDGMENT

Professor O. F. Nielsen and technician L. Ryelund, Department of Chemistry, University of Copenhagen are thanked for their assistance in obtaining the Raman spectra. This research was supported by the The Danish Council for Independent Research, Technology and Production Sciences (FTP).

REFERENCES

(1) Sjöström, E. *Wood Chemistry - Fundamentals and Applications*; 2nd ed.; Academic Press, Inc.: San Diego, CA, 1993.
(2) Whetten, R. W.; MacKay, J. J.; Sederoff, R. R. *Annu. Rev. Plant Physiol. Plant Mol. Biol.* **1998**, *49*, 585–609.
(3) Karkonen, A.; Koutaniemi, S. *J. Integr. Plant Biol.* **2010**, *52* (2), 176–185.
(4) Agarwal, U. P.; Atalla, R. H. *J. Wood Chem. Technol.* **1994**, *14* (2), 227–241.
(5) Atalla, R. H.; Agarwal, U. P. *J. Raman Spectrosc.* **1986**, *17* (2), 229–231.
(6) Agarwal, U. P.; Ralph, S. A. *Appl. Spectrosc.* **1997**, *51* (11), 1648–1655.
(7) Agarwal, U. P.; Landucci, L. L. *J. Pulp Pap. Sci.* **2004**, *30* (10), 269–274.
(8) Kihara, M.; Takayama, M.; Wariishi, H.; Tanaka, H. *Spectrochim. Acta A* **2002**, *58* (10), 2213–2221.
(9) Stewart, D.; Yahiaoui, N.; McDougall, G. J.; Myton, K.; Marque, C.; Boudet, A. M.; Haigh, J. *Planta* **1997**, *201* (3), 311–318.
(10) Barsberg, S.; Matousek, P.; Towrie, M.; Jorgensen, H.; Felby, C. *Biophys. J.* **2006**, *90* (8), 2978–2986.
(11) Saariaho, A. M.; Jaaskelainen, A. S.; Nuopponen, M.; Vuorinen, T. *Appl. Spectrosc.* **2003**, *57* (1), 58–66.
(12) Saariaho, A. M.; Argyropoulos, D. S.; Jaaskelainen, A. S.; Vuorinen, T. *Vib. Spectrosc.* **2005**, *37* (1), 111–121.
(13) Halttunen, M.; Vyorykka, J.; Hortling, B.; Tamminen, T.; Batchelder, D.; Zimmermann, A.; Vuorinen, T. *Holzforschung* **2001**, *55* (6), 631–638.
(14) Barsberg, S.; Matousek, P.; Towrie, M. S. *Macromol. Biosci.* **2005**, *5* (8), 743–752.
(15) Jaaskelainen, A. S.; Saariaho, A. M.; Vyorykka, J.; Vuorinen, T.; Matousek, P.; Parker, A. W. *Holzforschung* **2006**, *60* (3), 231–238.
(16) Larsen, K. L.; Barsberg, S.; Ronayne, K. L.; Parker, A. W.; Mateusek, P.; Towrie, M. Annual Report 2004−2005; Council for the Central Laboratory of the Research Councils: Chilton DIDCOT, 05.
(17) Vikkula, A.; Vuorinen, T. *J. Wood Sci.* **2007**, *53* (3), 229–233.
(18) Agarwal, U. P.; Reiner, R. S. *J. Raman Spectrosc.* **2009**, *40* (11), 1527–1534.
(19) Busch, S.; Schmitt, K.; Erhardt, C.; Speck, T. A *J. Raman Spectrosc.* **2010**, *41* (5), 490–497.
(20) Hohenberg, P.; Kohn, W. *Phys. Rev. B* **1964**, *136* (3B), B864–&.
(21) Kohn, W.; Sham, L. J. *Phys. Rev.* **1965**, *137* (6A), 1697–&.
(22) Becke, A. D. *J. Chem. Phys.* **1993**, *98* (2), 1372–1377.
(23) Lee, C. T.; Yang, W. T.; Parr, R. G. *Phys. Rev. B* **1988**, *37* (2), 785–789.
(24) Stephens, P. J.; Devlin, F. J.; Chabalowski, C. F.; Frisch, M. J. *J. Phys. Chem.* **1994**, *98* (45), 11623–11627.
(25) Vosko, S. H.; Wilk, L.; Nusair, M. *Can. J. Phys.* **1980**, *58* (8), 1200–1211.
(26) *Gaussian 03*, revision D.01; Gaussian, Inc: Wallingford, CT, 2004.
(27) Jalkanen, K. J.; Nieminen, R. M.; Frimand, K.; Bohr, J.; Bohr, H.; Wade, R. C.; Tajkhorshid, E.; Suhai, S. *Chem. Phys.* **2001**, *265* (2), 125–151.
(28) Jalkanen, K. J.; Suhai, S. *Chem. Phys.* **1996**, *208* (1), 81–116.
(29) Jalkanen, K. J.; Degtyarenko, I. M.; Nieminen, R. M.; Cao, X.; Nafie, L. A.; Zhu, F.; Barron, L. D. *Theor. Chem. Acc.* **2008**, *119* (1−3), 191–210.
(30) Frimand, K.; Bohr, H.; Jalkanen, K. J.; Suhai, S. *Chem. Phys.* **2000**, *255* (2−3), 165–194.
(31) Tajkhorshid, E.; Jalkanen, K. J.; Suhai, S. *J. Phys. Chem. B* **1998**, *102* (30), 5899–5913.
(32) Deng, Z.; Polavarapu, P. L.; Ford, S. J.; Hecht, L.; Barron, L. D.; Ewig, C. S.; Jalkanen, K. *J. Phys. Chem.* **1996**, *100* (6), 2025–2034.
(33) J.Koury; *Guide for Raman Shift Standards for Spectrometer Calibration in Annual Book ASTM Standards*; ASTM: West Conshohocken, PA, 1996; Vol. 0306.
(34) Mann, C. K.; Vickers, T. J. The Quest for Accuracy in Raman Spectra. In *Handbook of Raman Spectroscopy*, Lewis, I. R., Edwards, H. G. M., Eds.; Marcell Dekker, Inc: New York, 2001; pp 251−274.
(35) Larsen, K. L.; Barsberg, S. *J. Phys. Chem. B* **2010**, *114* (23), 8009–8021.
(36) Agache, C.; Popa, V. I. *Monatsh. Chem.* **2006**, *137* (1), 55–68.
(37) Andrade, S. G.; Goncalves, L. C. S.; Jorge, F. E. *J. Mol. Struct.-Theochem.* **2008**, *864* (1−3), 20–25.
(38) Avci, D.; Atalay, Y. *Int. J. Quantum Chem.* **2009**, *109* (2), 328–341.
(39) Finley, J. W.; Stephens, P. J. *J. Mol. Struct.-Theochem.* **1995**, *357* (3), 225–235.
(40) Merrick, J. P.; Moran, D.; Radom, L. *J. Phys. Chem. A* **2007**, *111* (45), 11683–11700.
(41) Pople, J. A.; Schlegel, H. B.; Krishnan, R.; Defrees, D. J.; Binkley, J. S.; Frisch, M. J.; Whiteside, R. A.; Hout, R. F.; Hehre, W. J. *Int. J. Quantum Chem.* **1981**, 269–278.
(42) Pople, J. A.; Scott, A. P.; Wong, M. W.; Radom, L. *Israel J. Chem.* **1993**, *33* (3), 345–350.
(43) Rauhut, G.; Pulay, P. *J. Phys. Chem.* **1995**, *99* (10), 3093–3100.
(44) Scott, A. P.; Radom, L. *J. Phys. Chem.* **1996**, *100* (41), 16502–16513.
(45) Sett, P.; Chattopadhyay, S.; Mallick, P. K. *Vib. Spectrosc.* **2009**, *49* (1), 84–95.
(46) Bouteiller, Y.; Gillet, J. C.; Gregoire, G.; Schermann, J. P. *J. Phys. Chem. A* **2008**, *112* (46), 11656–11660.
(47) Maes, G.; Smets, J.; Adamowicz, L.; McCarthy, W.; VanBael, M. K.; Houben, L.; Schoone, K. *J. Mol. Struct.* **1997**, *410*, 315–322.
(48) Palafox, M. A.; Rastogi, V. K.; Tanwar, R. P.; Mittal, L. *Spectrochim. Acta A* **2003**, *59* (11), 2473–2486.
(49) Palafox, M. A.; Tardajos, G.; Guerrero-Martinez, A.; Rastogi, V. K.; Mishra, D.; Ojha, S. P.; Kiefer, W. *Chem. Phys.* **2007**, *340* (1−3), 17–31.
(50) Borowski, P.; Fernandez-Gomez, M.; Fernandez-Liencres, M. P.; Ruiz, T. P. *Chem. Phys. Lett.* **2007**, *446* (1−3), 191–198.
(51) Borowski, P.; Pilorz, K.; Pitucha, M. *Spectrochim. Acta A* **2010**, *75* (5), 1470–1475.
(52) Vyas, N.; Ojha, A. K. *J. Mol. Struct.-Theochem* **2010**, *940* (1−3), 95–102.
(53) Pliego, J. R. *J. Mol. Catal. A: Chem.* **2005**, *239* (1−2), 228–234.
(54) Improta, R.; Benzi, C.; Barone, V. *J. Am. Chem. Soc.* **2001**, *123* (50), 12568–12577.
(55) Barsberg, S. *Int. J. Quantum Chem.* **2009**, *109* (7), 1531–1546.
(56) Cappelli, C.; Corni, S.; Cammi, R.; Mennucci, B.; Tomasi, J. *J. Chem. Phys.* **2000**, *113* (24), 11270–11279.

(57) Cappelli, C.; Silva, C. O.; Tomasi, J. *J. Mol. Struct.-Theochem* **2001**, *544*, 191–203.
(58) Corni, S.; Cappelli, C.; Cammi, R.; Tomasi, J. *J. Phys. Chem. A* **2001**, *105* (36), 8310–8316.
(59) Corni, S.; Cappelli, C.; Del Zoppo, M.; Tomasi, J. *J. Phys. Chem. A* **2003**, *107* (48), 10261–10271.
(60) ElAzhary, A. A.; Suter, H. U. *J. Phys. Chem.* **1996**, *100* (37), 15056–15063.